NANO LETTERS

pubs.acs.org/NanoLett

Nanomanipulation Using Silicon Photonic Crystal Resonators

Sudeep Mandal,[†] Xavier Serey,[†] and David Erickson*[,‡]

[†]School of Applied and Engineering Physics, Cornell University, Ithaca, New York 14853 and [‡]Sibley School of Mechanical and Aerospace Engineering, Cornell University, Ithaca, New York 14853

ABSTRACT Optical tweezers[1] have enabled a number of microscale processes such as single cell handling[2], flow-cytometry,[3] directed assembly,[4,5] and optical chromatography.[6,7] To extend this functionality to the nanoscale, a number of near-field approaches have been developed that yield much higher optical forces by confining light to subwavelength volumes.[8−10] At present, these techniques are limited in both the complexity and precision with which handling can be performed. Here, we present a new class of nanoscale optical trap exploiting optical resonance in one-dimensional silicon photonic crystals. The trapping of 48 nm and 62 nm dielectric nanoparticles is demonstrated along with the ability to transport, trap, and manipulate larger nanoparticles by simultaneously exploiting the propagating nature of the light in a coupling waveguide[11] and its stationary nature within the resonator. Field amplification within the resonator is shown to produce a trap several orders of magnitude stronger than conventional tweezers and an order of magnitude stiffer than other near-field techniques. Our approach lays the groundwork for a new class of optical trapping platforms that could eventually enable complex all-optical single molecule manipulation and directed assembly of nanoscale material.

Since Arthur Ashkin's pioneering work[12] on laser-induced optical trapping and the manipulation of micrometer-sized dielectric microspheres, optical tweezers have developed into an invaluable tool for a variety of applications such as flow cytometry,[2,3] single-molecule studies,[13,14] and optical chromatography.[6,7] The interest in optical tweezers lies in their ability to precisely and noninvasively manipulate particles and to decouple their motion from that of the ambient background (for example a flow within a microfluidic environment). Recently demonstrated indirect optical methods[15] have enabled a similar level of control with significantly lower optical power requirements. Researchers have also demonstrated easy fabrication of well-calibrated optical traps in an integrated, microfluidic system by incorporating Fresnel zone plates.[16] However, in all these methods diffraction limits how tightly light can be focused which in turn limits the ultimate strength of the optical trap and by extension the size of the matter which can be manipulated.

Recently, researchers have demonstrated the ability to surpass the limits imposed by free-space diffraction by tailoring the optical and structural properties of a medium.[10,17,18] For example, Grigorenko et al.[8] utilized the strongly enhanced and localized optical near-fields of closely spaced metallic nanostructures. Similarly Yang et al.[9] were able to demonstrate optical trapping and transport of dielectric nanoparticles by exploiting the strong field confinement within slot waveguides.[19] While the strength of optical traps can be enhanced by the strong confinement of the optical field, it can also be improved by exploiting the field amplification within an optical resonator. Recently, Arnold et al.[20] demonstrated the trapping and transport of polystyrene nanoparticles as small as 280 nm in diameter in a circular orbit around whispering gallery mode (WGM) resonators possessing Q-factors as high as 10^6.

Here, we present a new class of resonant optical traps that are capable of generating extremely strong optical field gradients in three dimensions while simultaneously enhancing the trap stiffness due to the amplification of the optical field within the resonator and enabling advanced particle handling functionalities. As illustrated in Figure 1a, our optical trap consists of a one-dimensional silicon photonic crystal resonator that is evanescently coupled to a single mode waveguide. The standing wave nature of the resonant optical field within the resonator enables a true static point trap with strong field confinement in all three dimensions. An SEM image of a typical resonator is shown in supplementary Figure S1 and the fabrication procedure is described in the Supporting Information.

When light at the resonant wavelength is coupled into the bus-waveguide, a stationary interference pattern is formed within the photonic crystal resonator resulting in a tight confinement of the optical field in an extremely small volume as illustrated in Figure 1b. These strong field gradients coupled with the resonant amplification of the optical field within the resonator enables the stable trapping of particles ranging in size from 50 to 500 nm. Figure 2 (also see Movie 1in Supporting Information) shows the trapping and release of a 62 nm polystyrene nanoparticle (refractive index $n = 1.59$). As can be seen in the supplementary movie, we were also able to trap polystyrene nanoparticles that were 48 nm in diameter. We note that both of these targets are well below the size limit of what could be trapped using previous approaches.[19] A tunable infrared laser was used to couple TE polarized light at the resonant wavelength of 1548.15 nm into the input end of the waveguide using a

Received for review: 09/4/2009
Published on Web 00/00/0000

DOI: 10.1021/nl9029225 | *Nano Lett.* **XXXX,** *xxx,* 000-000

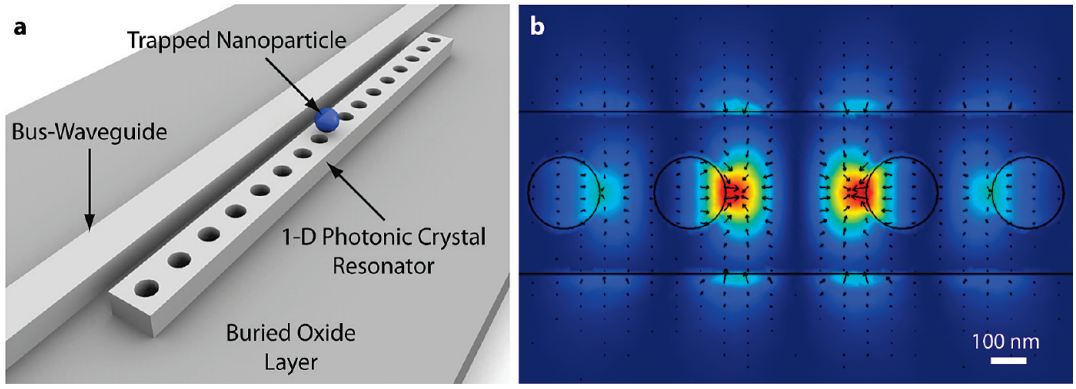

FIGURE 1. Photonic crystal resonator for enhanced optical trapping. (a) 3D schematic of the one-dimensional photonic crystal resonator optical trapping architecture (b) 3D FEM simulation illustrating the strong field confinement and amplification within the one-dimensional resonator cavity. The black arrows indicate the direction and magnitude of the local optical forces.

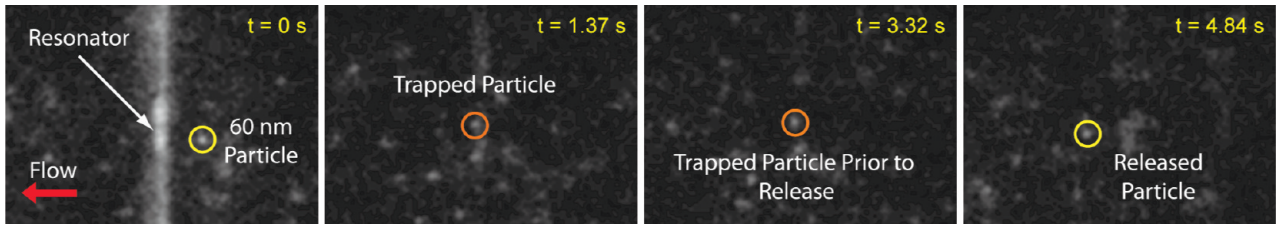

FIGURE 2. Trapping of nanoparticles on photonic crystal resonator. Movie showing the capture and subsequent release of 62 and 48 nm diameter polystyrene nanoparticles is included in the Supporting Information (supplementary movie 1). In this figure the waveguide is excited at the resonant wavelength while 62 nm particles flow through a microfluidic channel running over the resonator and the waveguide. The sequence of images was captured by a Hamamatsu CCD camera with contrast and brightness adjustments applied to the entire image. The yellow circle tracks the 62 nm particle which is trapped (indicated by orange circles) on the resonator. Turning the laser power off releases the particle from the trap.

lensed fiber. The output power at the waveguide exit was measured to be 1.7 mW. In the experiment a microfluidic flow convects the particles along the channel and toward the resonator. If a particle passes within close proximity of the resonator surface and the resonant optical field lobes, it experiences a tweezing force due to the strong local field gradient resulting in the particle getting trapped at the resonator surface. The trapped particle is subsequently released by turning the laser power off (as is shown for the 62 nm case above). Trapped particles can also be released either by detuning the input wavelength away from resonance or by switching the polarization of light from TE to TM.

One interesting aspect of our optical trap design is that the guided optical mode within the waveguide possesses a forward momentum which enables the simultaneous trapping and propulsion of nanoparticles along its surface.[11,21,22] In contrast, at resonance, the field within the optical resonator consists of a tightly confined standing wave with no propagation component. By tailoring the microfluidic flow and exploiting this contrasting nature of the optical field within the waveguide and the one-dimensional resonator, we demonstrate a novel technique for performing particle manipulations.

Figure 3 (see also supplementary movie 2) illustrates a series of time-lapse images demonstrating the trapping and manipulation of 500 nm polystyrene microspheres. In the top panel of Figure 3 the flow in the microfluidic channel is from left to right. A 500 nm polystyrene microsphere is trapped and transported along the waveguide by the evanescent field of the guided optical mode. The input light is initially tuned to the resonant wavelength. As a result, when the particle moves up along the waveguide and approaches the resonator, it experiences a lateral tweezing force toward the resonator center. Due to the field amplification within the resonator and the stronger field gradients in the photonic crystal structure, the lateral tweezing force experienced by the particle is much stronger than the trapping force exerted by the waveguide. This results in the particle hopping from the waveguide to the resonator center. Once trapped, the particle is held stationary on the resonator. To release the particle back onto the waveguide, the input wavelength is tuned away from resonance. This releases the particle from the resonator trap, and it is convected with the fluid flow toward the waveguide. Since the waveguide is not wavelength selective, the evanescent field of the off-resonant guided optical mode retraps the particle as it passes above its surface. Once the particle is trapped on the waveguide,

DOI: 10.1021/nl9029225 | *Nano Lett.* **XXXX,** *xxx,* 000-000

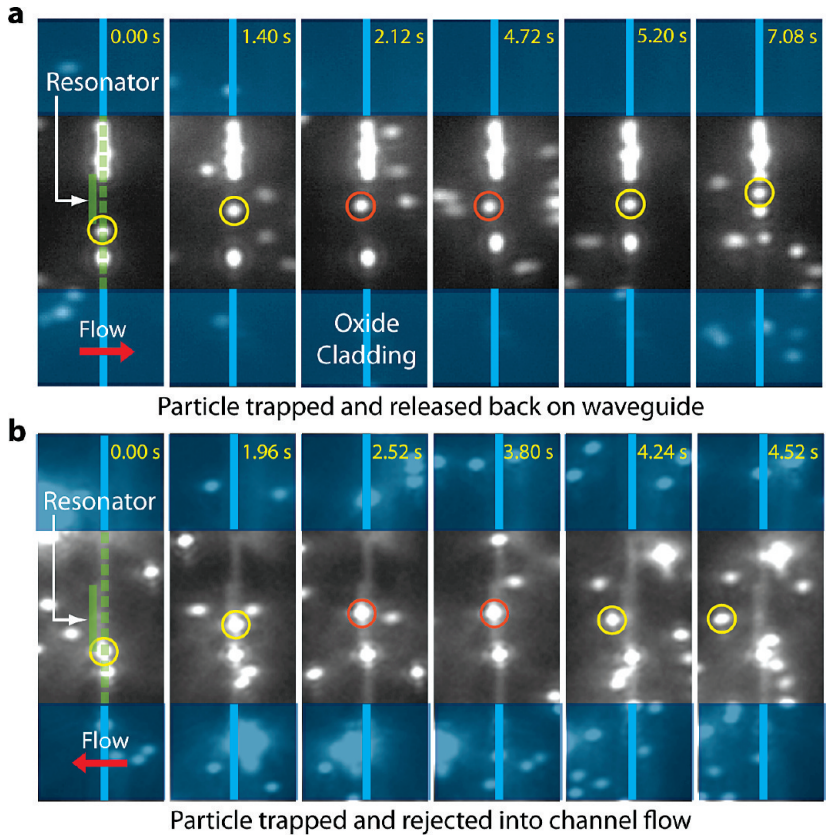

FIGURE 3. Particle handling and manipulation using photonic crystal resonators. Movie illustrating the trapping and subsequent handling of 500 nm polystyrene nanoparticles is included in the Supporting Information (supplementary movie 2). (a) The waveguide is excited at the resonant wavelength with the guided mode propagating upward (in the figure). A 500 nm particle is trapped on the waveguide (yellow circle) and is transported toward the resonator. When the particle arrives in the vicinity of the resonator center, it hops from the waveguide onto the resonator center and remains trapped on the resonator (orange circles). Since the flow is from left to right, detuning the input wavelength away from resonance releases the particle from the resonator and back onto the waveguide after which it continues to be transported upward along the waveguide. (b) By simply reversing the direction of flow in the microfluidic channel, the particle can be rejected into the fluidic channel after it is initially transported and trapped at the resonator center.

it is subsequently transported further along the waveguide. When the direction of flow in the microchannel is reversed (Figure 3b), the trapped particle on the resonator can be rejected into the fluid flow when the input laser is tuned off-resonance.

To characterize the trapping stiffness as well as the maximum trapping force in all three dimensions in our system, we have carried out a detailed three-dimensional finite element numerical analysis using a commercial software package (COMSOL). The material properties of the silicon resonator and the surrounding water medium were taken into consideration while solving for the electromagnetic field distribution at resonance. To determine the force exerted on a particle, we construct a virtual spherical surface that encloses the particle and calculate the electromagnetic field on this surface. By evaluating the time-independent Maxwell stress tensor and integrating it over the closed surface enclosing the particle, we are able to obtain the trapping force. Figure 4 illustrates the trapping force profile for a 100 nm polystyrene microsphere that is displaced in all three dimensions from the stable trapping position for 1 W of input power. We observe that the maximum trapping force for a 100 nm particle is 700 pN (evaluated 25 nm from the resonator surface) which is more than an order of magnitude higher than the maximum trapping force in the case of slot waveguides[9] (25 pN). The required placement of a Maxwell stress tensor surface around the particle as well as numerical meshing limitations prevented the calculation of forces when the particle was closer than 25 nm from the resonator surface. A common figure of merit related to the quality of optical traps is the trap stiffness for a given particle size. From Figure 4 we estimate a trap stiffness of 4.81, 3.30, and 8.53 pN nm^{-1} W^{-1} for a 100 nm polystyrene microsphere along the X, Y, and Z axes, respectively, corresponding to a radial trap stiffness (in the $X-Y$ plane) of 1.96 pN nm^{-1} W^{-1}.

To obtain experimental values for the trapping stiffness in the X and Y axis and compare them with theoretical estimates, the suppressed Brownian motion of a trapped 200 nm particle was studied. Triton X-100 (1%) was used as a surfactant to minimize stiction between the nanoparticle and the resonator surface. Figure 5 illustrates a scatter plot of the position trace of a 200 nm particle when the output power measured at the waveguide output was 140 μW. The

DOI: 10.1021/nl9029225 | *Nano Lett.* **XXXX,** *xxx,* 000-000

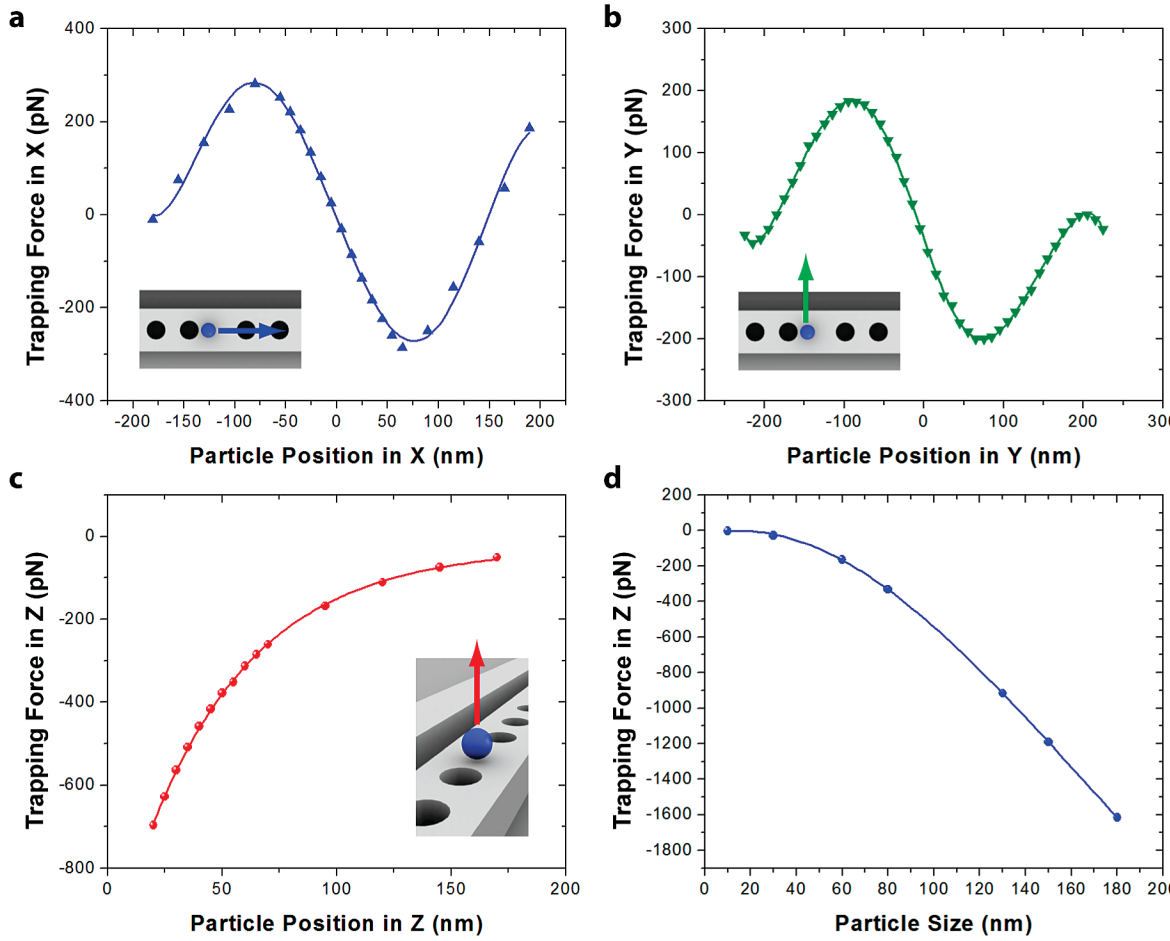

FIGURE 4. Numerical analysis of trapping forces. All computed trapping forces listed are normalized to 1 W of input power in the waveguide.(a) Force experienced by a 100 nm trapped polystyrene nanoparticle as it is displaced along the length of the resonator (*X*-axis). The zero *X*-axis value corresponds to the stable trapping position at the lobe center. The linear nature of the plot of the restoring force in the *X*-axis indicates a Hookean behavior over a displacement of approximately 75 nm from the stable trapping position. (b) Graph illustrating the restoring force on a 100 nm particle as it is displaced in the *Y*-axis, normal to the length of the resonator. The zero *Y*-axis value corresponds to the stable trapping position at the lobe center. Similar to the displacement in the *X*-axis, the restoring force indicates a Hookean behavior for displacements of approximately 75 nm from the equilibrium trapping position. (c) Plot of the trapping force in the *Z*-direction as the particle is moved away from the resonator surface. The zero *Z*-axis value corresponds to the particle being in contact with the resonator surface. Due to the exponential nature of decay of the optical field in the *Z*-direction, the force is also observed to decay exponentially. (d) Graph shows the magnitude of the maximum trapping force in the *Z*-direction as a function of particle size. Particle position is 25 nm above the stable trapping position. We observe that forces over 1 nN can be exerted on dielectric particles as small as 135 nm with this resonant photonic crystal architecture. Plots a, b, and d were evaluated 25 nm above the surface of the sensor.

scatter plot is overlaid on top of the field distribution within the resonator (to scale). It is evident that at such low optical powers, the trap is weak and the particle hops between the two center lobes of the resonant optical field. We also observe that the particle hops to the weaker traps at the side lobes for a short duration of time. When the power is raised such that the measured power at the waveguide output is 175 μW, the strength of the trap increases and the particle is observed to remain stably trapped at a single site. Parts c and d of Figure 5 show histograms for the displacement of a trapped 200 nm particle which exhibits a Gaussian distribution. From these plots, we are able to determine a radial trapping stiffness of 2.86 pN nm^{-1} W^{-1}, which is slightly lower than our numerical estimate of 5.38 pN nm^{-1} W^{-1} for a 200 nm particle (see Supporting Information section II and supplementary Figure S2). Since the experimentally observed trap stiffness agrees reasonably well with our numerical estimates, we can infer that surface interactions between the particle and the resonator surface do not dominate the trapping characteristics. In general, we observe a higher trap stiffness for larger particles as they are influenced by a larger portion of the optical field.

The estimated trapping stiffness for this system is an order of magnitude higher than that of slot waveguides (0.2 pN nm^{-1} W^{-1} for a 100 nm particle[9]) and several orders of magnitude higher than other recent optical trapping techniques such as plasmonic tweezers[8] (0.013 pN nm^{-1} W^{-1} for a 200 nm bead), conventional high-NA optical tweezers[23] (0.16 pN nm^{-1} W^{-1} for a 500 nm bead), and Fresnel zone plate optical tweezers[16] (0.1 pN nm^{-1} W^{-1} for a 2 μm bead).

DOI: 10.1021/nl9029225 | *Nano Lett.* **XXXX,** *xxx,* 000-000

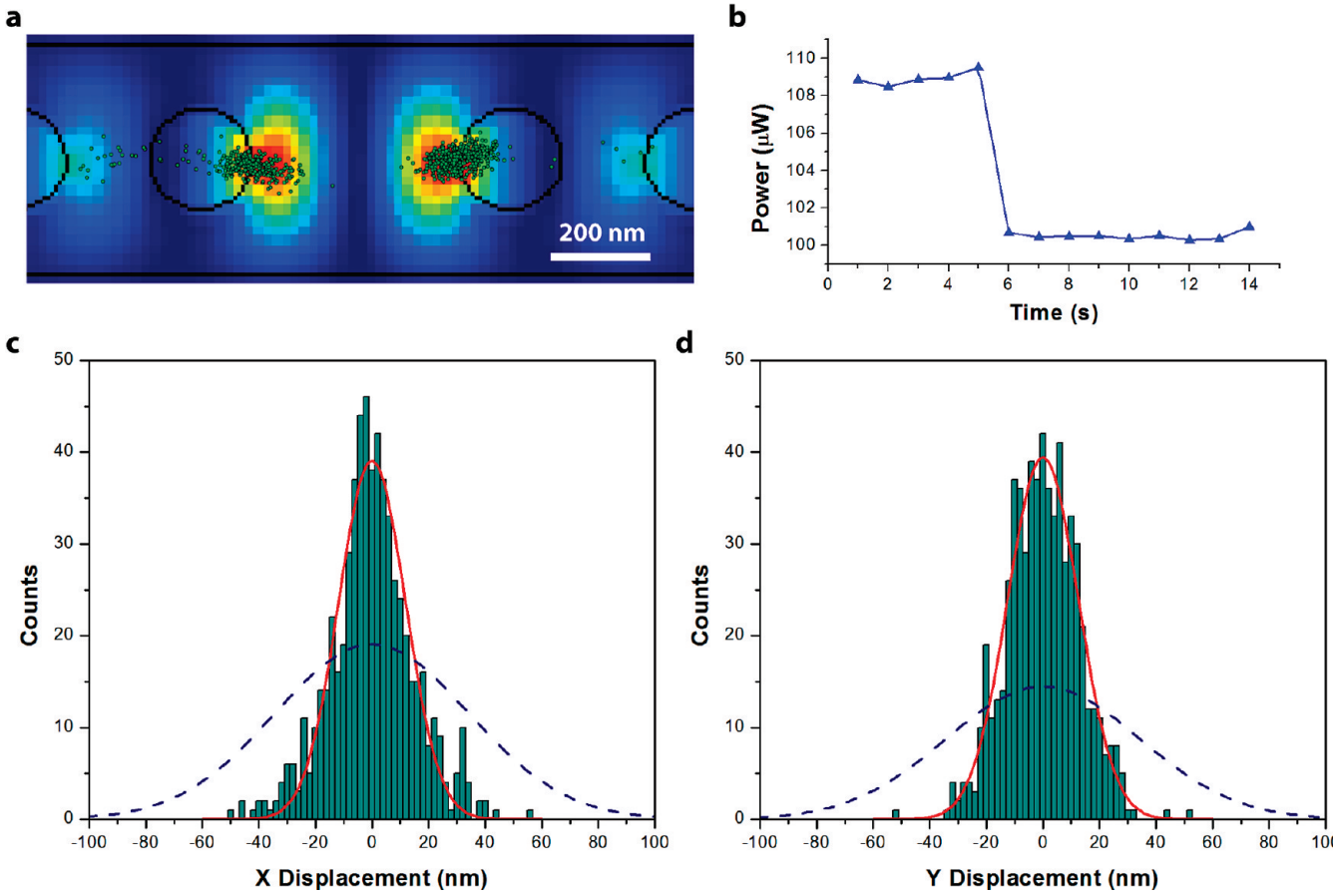

FIGURE 5. Trapping stiffness and the suppression of Brownian motion. (a) The plot shows the Brownian motion a 200 nm particle when the measured light output at the end of the waveguide was 140 μW. The particle is observed to hop between the two center lobes in the resonant cavity. The nanoparticle is also observed to hop for a brief duration to the weaker optical lobes adjacent to the central lobes within the resonant cavity. (b) The release of a particle from a trap can be inferred by monitoring the output power of the waveguide for discrete jumps in the power level. In the case of 200 nm particles, the release of the particle induces a slight shift in the resonant wavelength of the cavity. This shift can be detected as a discrete jump in the output power at the end of the waveguide. This graph illustrates this concept by demonstrating a drop in the output power of the waveguide when the 200 nm particle escapes from the optical trap. (c and d) Histograms showing the Brownian motion of a trapped 200 nm particle in the X and Y directions at a single optical lobe (output power = 175 μW). The histograms follow a Gaussian distribution and are used to experimentally estimate the trapping stiffness of the optical traps. The blue dashed curves represent the true Gaussian fit for the Brownian motion after correcting for video motion-blur (see Supporting Information).

While it is difficult to make a clear comparison between these different trapping techniques due to the dependence of the trapping stiffness on particle size, it is evident that the strength of our optical trap exceeds the state-of-the-art by at least an order of magnitude.

The presence of a trapped particle affects the resonant wavelength of the resonator by a small amount. Thus, when a trapped particle escapes from the trap, it induces a slight shift in the resonant wavelength which manifests itself as a discrete jump in the output power from the waveguide. By monitoring the laser power at the output end of the waveguide, it is possible to infer the release of a particle from the optical trap as shown in Figure 5b. It is important to note that this effect is more pronounced in the case of larger nanoparticles.[24,25] As the size of the particle reduces, the induced shift in the resonant wavelength also decreases.

We have previously demonstrated the capability of this resonator design to perform multiplexed biomolecular detections.[26] This, coupled with its ability to optically transport nanoparticles along trajectories independent of the microfluidic channel flow and trap, store, and reject them, opens up exciting possibilities in creating a robust integrated system for the simultaneous probing, detection, and handling of biomolecules. An important aspect of this new trapping system is the ability to further improve upon the trapping capabilities by tuning the design geometry.[27] In our current experiments the Q-factor of our resonator was approximately 2500 in water. However, researchers have recently demonstrated the ability to achieve Q-factors higher than 10^7 using similar one-dimensional photonic crystal geometries.[28−30] Although these improved Q-factors have been demonstrated for air clad resonators, it should be possible to employ similar techniques to tailor the water-clad resonator geometries to achieve high Q-factors. In addition, fabricating silicon nitride resonators[31] that resonate at visible wavelengths can help minimize absorption

DOI: 10.1021/nl9029225 | *Nano Lett.* **XXXX,** *xxx,* 000-000

of light by water thus providing another means for improving the *Q*-factor of these water-clad devices. While other optical resonator designs possessing higher *Q*-factors have been previously demonstrated,[20,32] they are not as well suited for trapping applications due to their larger mode volumes, weaker field gradients, and propagating nature of their guided optical mode that prevents the static trapping of nanoparticles. Future work focused on the development of high-*Q* photonic crystal resonator traps will enable further improvements in trapping capabilities, thus opening us up to the realm of single-molecule optical trapping.

SUPPORTING INFORMATION AVAILABLE

Experimental methods and additional details regarding the estimation of the optical trap stiffness are provided. Movie 1 illustrates the trapping of 48 and 62 nm polystyrene nanoparticles, and movie 2 demonstrates the ability to perform advanced handling operations on 500 nm nanoparticles. This material is available free of charge via the Internet at http://pubs.acs.org.

AUTHOR INFORMATION

Corresponding Author

* To whom correspondence should be addressed, E-mail: de54@cornell.edu.

Acknowledgment. We thank M. Lipson, A. Nitkowski, S. Moore, and A. H. J. Yang (Cornell) for technical discussions. This work was supported by the Nanobiotechnology Center (NBTC), an STC Program of the National Science Foundation under Agreement No. ECS-9876771, the National Institutes of Health—National Institute of Biomedical Imaging and Bioengineering (NIH-NIBIB) under Grant Number R21EB007031, and the US National Science Foundation through the NIRT: Active Nanophotofluidic Systems for Single Molecule/Particle Analysis grant CBET-0708599. Device fabrication for this work was performed in part at the Cornell NanoScale Facility, a member of the National Nanotechnology Infrastructure Network, which is supported by the National Science Foundation. Video Spot Tracker software package by CISMM at UNC—CH was supported by the NIH-NIBIB (NIH 5-P41-RR02170).

REFERENCES AND NOTES

(1) Grier, D. G. *Nature* **2003**, *424*, 810–816.
(2) MacDonald, M. P.; Spalding, G. C.; Dholakia, K. *Nature* **2003**, *426*, 421–424.
(3) Wang, M. M.; Tu, E.; Raymond, D. E.; Yang, J. M.; Zhang, H. C.; Hagen, N.; Dees, B.; Mercer, E. M.; Forster, A. H.; Kariv, I.; Marchand, P. J.; Butler, W. F. *Nat. Biotechnol.* **2005**, *23*, 83–87.
(4) Jamshidi, A.; Pauzauskie, P. J.; Schuck, P. J.; Ohta, A. T.; Chiou, P.-Y.; Chou, J.; Yang, P.; Wu, M. C. *Nat. Photonics* **2008**, *2*, 86–89.
(5) Agarwal, R.; Ladavac, K.; Roichman, Y.; Yu, G.; Lieber, C.; Grier, D. *Opt. Express* **2005**, *13*, 8906–8912.
(6) Terray, A.; Arnold, J.; Hart, S. J. *Opt. Express* **2005**, *13*, 10406–10415.
(7) Imasaka, T. *Analusis* **1998**, *26*, M53–M55.
(8) Grigorenko, A. N.; Roberts, N. W.; Dickinson, M. R.; ZhangY., *Nat. Photonics* **2008**, *2*, 365–370.
(9) Yang, A. H. J.; Moore, S. D.; Schmidt, B. S.; Klug, M.; Lipson, M.; Erickson, D. *Nature* **2009**, *457*, 71–75.
(10) Reece, P. J.; Garces-Chavez, V.; Dholakia, K. *Appl. Phys. Lett.* **2006**, 88.
(11) Gaugiran, S.; Getin, S.; Fedeli, J. M.; Colas, G.; Fuchs, A.; Chatelain, F.; Derouard, J. *Opt. Express* **2005**, *13*, 6956–6963.
(12) Ashkin, A. *Phys. Rev. Lett.* **1970**, *24*, 156–159.
(13) Moffitt, J. R.; Chemla, Y. R.; Aathavan, K.; Grimes, S.; Jardine, P. J.; Anderson, D. L.; Bustamante, C. *Nature* **2009**, *457*, 446–450.
(14) Ferrer, J. M.; Lee, H.; Chen, J.; Pelz, B.; Nakamura, F.; Kamm, R. D.; Lang, M. J. *Proc. Natl. Acad. Sci. U.S.A.* **2008**, *105*, 9221–9226.
(15) Chiou, P. Y.; Ohta, A. T.; Wu, M. C. *Nature* **2005**, *436*, 370–372.
(16) Schonbrun, E.; Rinzler, C.; Crozier, K. B. *Appl. Phys. Lett.* **2008**, *92*, 071112–3.
(17) Fang, N.; Lee, H.; Sun, C.; Zhang, X. *Science* **2005**, *308*, 534–537.
(18) Volpe, G.; Quidant, R.; Badenes, G.; Petrov, D. *Phys. Rev. Lett.* **2006**, *96*, 238101–4.
(19) Almeida, V. R.; Xu, Q. F.; Barrios, C. A.; Lipson, M. *Opt. Lett.* **2004**, *29*, 1209–1211.
(20) Arnold, S.; Keng, D.; Shopova, S. I.; Holler, S.; Zurawsky, W.; Vollmer, F. *Opt. Express* **2009**, *17*, 6230–6238.
(21) Schmidt, B. S.; Yang, A. H.; Erickson, D.; Lipson, M. *Opt. Express* **2007**, *15*, 14322–14334.
(22) Kawata, S.; Sugiura, T. *Opt. Lett.* **1992**, *17*, 772–774.
(23) Neuman, K. C.; Block, S. M. *Rev. Sci. Instrum.* **2004**, *75*, 2787–2809.
(24) Barth, M.; Benson, O. *Appl. Phys. Lett.* **2006**, *89*, 253114–3.
(25) Vollmer, F.; Arnold, S.; Keng, D. *Proc. Natl. Acad. Sci. U.S.A.* **2008**, *105*, 20701–20704.
(26) Mandal, S.; Goddard, J. M.; Erickson, D. *Lab Chip* **2009**, *9*, 2924–2932.
(27) Lin, S.; Hu, J.; Kimerling, L.; Crozier, K. *Opt. Lett.* **2009**, *34*, 3451–3453.
(28) Velha, P.; Rodier, J. C.; Lalanne, P.; Hugonin, J. P.; Peyrade, D.; Picard, E.; Charvolin, T.; Hadji, E. *Appl. Phys. Lett.* **2006**, *89*, 171121–3.
(29) Notomi, M.; Kuramochi, E.; Taniyama, H. *Opt. Express* **2008**, *16*, 11095–11102.
(30) Deotare, P. B.; McCutcheon, M. W.; Frank, I. W.; Khan, M.; Loncar, M. *Appl. Phys. Lett.* **2009**, *94*, 121106–3.
(31) McCutcheon, M. W.; Loncar, M. *Opt. Express* **2008**, *16*, 19136–19145.
(32) Armani, D. K.; Kippenberg, T. J.; Spillane, S. M.; Vahala, K. J. *Nature* **2003**, *421*, 925–928.

DOI: 10.1021/nl9029225 | *Nano Lett.* **XXXX,** *xxx,* 000-000